EXPERIMENTAL STUDY ON A CLOSED-CONDUIT FLOW PERTURBED BY A TWO-DIMENSIONAL HILL

Henrique Pelisson Chimetta, henriquepc@fem.unicamp.br[1]
Erick de Moraes Franklin, franklin@fem.unicamp.br[1]

[1]Faculty of Mechanical Engineering - UNICAMP, Rua Mendeleyev, 200, Campinas - SP, 13083-860, Brazil

Abstract: *We present here some results of an experimental study on the perturbation of a fully developed turbulent boundary layer by a two-dimensional asymmetric hill of low aspect ratio $O(0.1)$. In our experiments, water flows were imposed over an asymmetric hill, with a relatively small curvature, fixed on the bottom wall of a closed conduit. Particle image velocimetry (PIV) was used to measure the flow fields. For the flow upstream of the hill, we found some usual characteristics of a turbulent channel flow, such as logarithmic regions and typical profiles of the xy component of the Reynolds stress. Over the ripple, the maximum of the vertical component of the mean velocity is restricted to a narrow band, above the ripple surface, for every longitudinal position toward the crest. We found the region where the Reynolds stress is perturbed, and the turbulent kinetic energy production was also computed.*
Keywords: *Boundary-layer, Perturbation, Low hill*

1. INTRODUCTION

Perturbations in boundary layers are frequently encountered in nature and industry. Some examples are airflows over hills, water flows over river dunes, and liquid flows over sand ripples and dunes in closed conduits such as petroleum pipelines. With the boundary layer perturbed, the distributions of velocities and stresses change along the flow. These new distributions are important to understand the bed instabilities associated with sediment transport (Franklin, 2010; Franklin, 2011 and Franklin, 2012) for example.

Some previous studies on this subject are based on asymptotic methods, where the turbulent boundary layer over a hill of small aspect ratio is divided into two regions, which can be used to determined the perturbed flow (Belcher and Hunt, 1998 and Jackson and Hunt, 1975). In the case of high Reynolds numbers, the inner region, close to the bed, is in local equilibrium because the timescale for the dissipation of the energy-containing eddies is much smaller than the timescale for their advection, allowing the use of models for turbulent stresses. For the outer region, the timescale for the dissipation of the energy-containing eddies is much larger than the timescale for their advection; therefore, the flow is not in local equilibrium.

Franklin and Ayek (2013) showed that the inner regions of the perturbed closed-conduit flow are not in local equilibrium in case of moderate Reynolds numbers ($\sim 10^4$), at least for a two-dimensional hill with triangular shape. This happens because of the relatively large ratio between the vertical and longitudinal flow scales (when compared with the aeolian case). This means that the asymptotic expressions for the perturbed boundary layer based on local equilibrium conditions must be used with care in case of aquatic ripples of triangular shape.

This study presents some results of an experimental study on the perturbation of a turbulent boundary layer by a two-dimensional hill. Closed-conduit water flows were imposed over an asymmetric hill with aspect ratio $O(0.1)$, and the flow was measured by particle image velocimetry (PIV). The mean velocities and fluctuations were computed from the acquired images, so that the shear stress over the ripple could be determined.

2. EXPERIMENTAL SETUP

The experimental device consisted basically of a water reservoir, two centrifugal pumps with bronze impeller and volute, a flow straightener, a 5-m long transparent channel of rectangular cross section (160-mm wide by 50-mm high), a settling tank and a return line, so that the water flowed in a closed loop.

The straightener consisted of a divergent-convergent nozzle filled with 3 mm diameter glass spheres, whose function was to homogenize the flow profile, and it was placed at the channel inlet. Following the divergent-convergent nozzle, the channel consisted of a 3-m-long section with flat walls until the beginning of the test section, which was 1-m long. The settling tank and the return line were connected to the test section exit by another 1-m long section. Figure 1 represents a schematic drawing of the experimental device.

We used PVC plates of 7-mm thickness to cover the entire bottom of the channel in order to reduce the height and facilitate the handling of the ripple. To model the two-dimensional ripple, a small bedform of wave shape was fixed on a PVC plate in the test section. The wave bedform had the same scales as the aquatic ripples (Franklin and Charru, 2009; Franklin, 2010 and Franklin, 2011). The bedform, of PVC, was painted in black to minimize undesirable reflections. Figure 2 presents the dimensions (in mm) of the wave bedform.

The employed flow rates were 8 and 10 m^3/h. These flow rates corresponded to cross-sectional mean velocities $\bar{U}$ of 0.32 and 0.40 m/s and to Reynolds numbers Re = $\bar{U}2H_{eff}/\nu$ of 2.75×10^4 and 3.5×10^4, where H_{eff} is the distance from the surface of the PVC plates to the top wall of the channel.

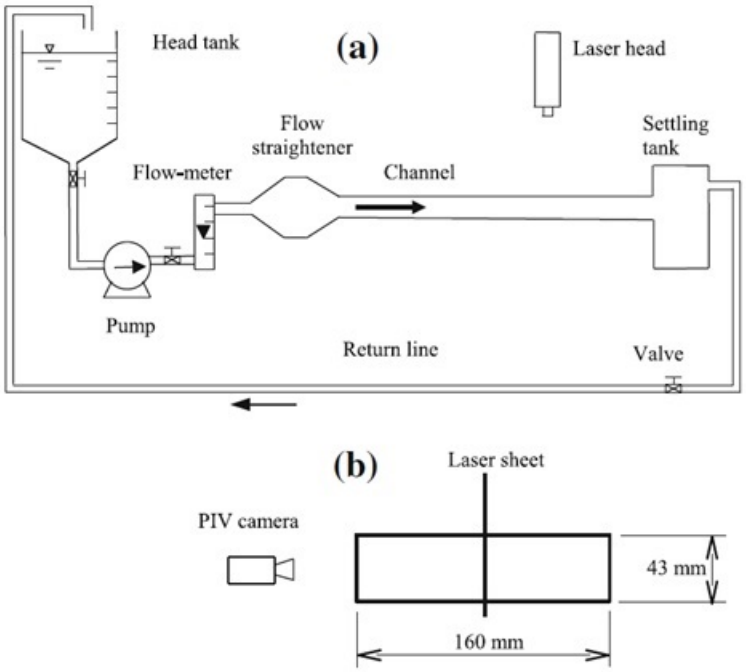

Figura 1: **Layout of the experimental device: (a) side view; (b) cross section. Figure extracted from Franklin and Ayek (2013)**

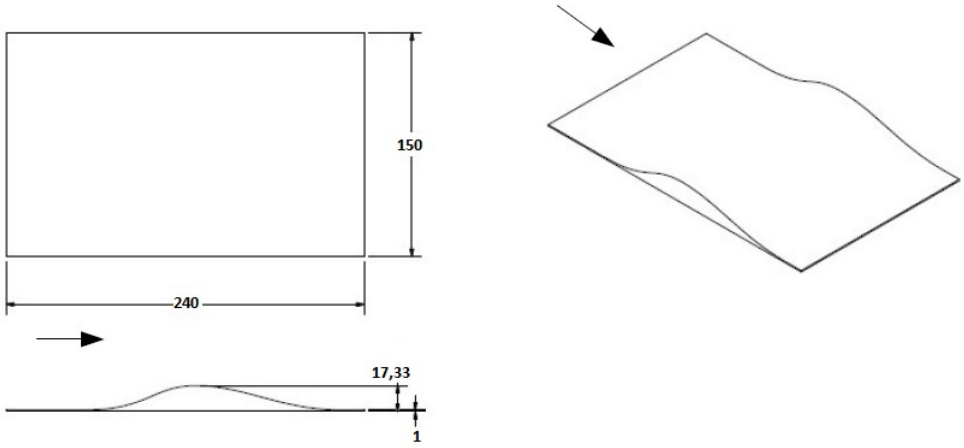

Figura 2: **Wave bedform employed as a model ripple (in the figure, the flow direction is indicated by the arrow)**

To obtain the instantaneous velocity fields of the flow we used PIV. The employed light source was a dual cavity Nd:YAG Q-Switched laser, capable of emitting 2 $\times$ 130 mJ at 15-Hz. The power of the laser was fixed at 66 % of the maximum power to assure a good balance between the image contrasts and undesirable reflection from the channel walls. 10-μm hollow glass beads (S.G. = 1.05) were employed as seeding particles.

To capture the images we used a 7.4-μm $\times$ 7.4-μm (px^2) CCD (charge coupled device) camera with a spatial resolution of 2,048 px $\times$ 2,048 px and acquiring pairs of images at 4 Hz. The total field employed was of 140 mm $\times$ 140 mm, corresponding to a magnification of 0.1, and the employed interrogation area was of 16 px $\times$ 16 px, corresponding to 0.12 mm $\times$ 0.12 mm. The computations were made with 50 % of overlap, corresponding to 256 interrogation areas.

The test section was divided in five parts, for each part were acquired 3,000 pairs of images for both flow rates, from which the fields of instantaneous velocity were computed in fixed Cartesian grids by the PIV controller software. Matlab scripts were written to post-process these fields. Figure 3 presents an example of PIV image (for one of the five parts) for the experiments with the ripple.

3. RESULTS

3.1 Channel flow

The flow was measured in five different parts, the first one was upstream of the bedform. In this part, the flow corresponded to a fully-developed turbulent channel flow. This region is indicated in the following by the subscript

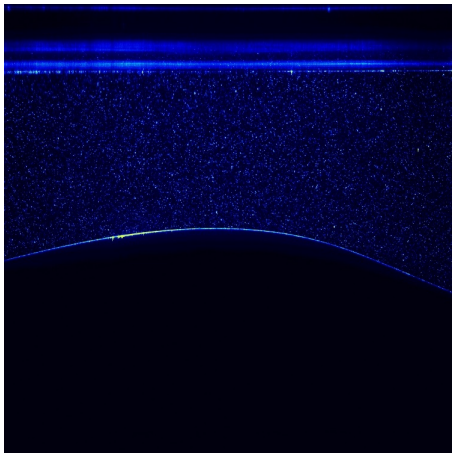

Figura 3: **Image of a PIV experiment in the presence of a ripple. In this image, the flow is from *right* to *left***

0. Using Matlab, the instantaneous fields were time average and the second-order moments (fluctuation fields) were computed and time averaged. The time-averaged fields were then space averaged in the longitudinal direction because the flow was fully developed. Figure 4 shows the profiles of the longitudinal component of the mean velocities. The profiles were slightly asymmetric. This was expected because the channel has a top-bottom asymmetry due the PVC plates placed in the bottom of the channel.

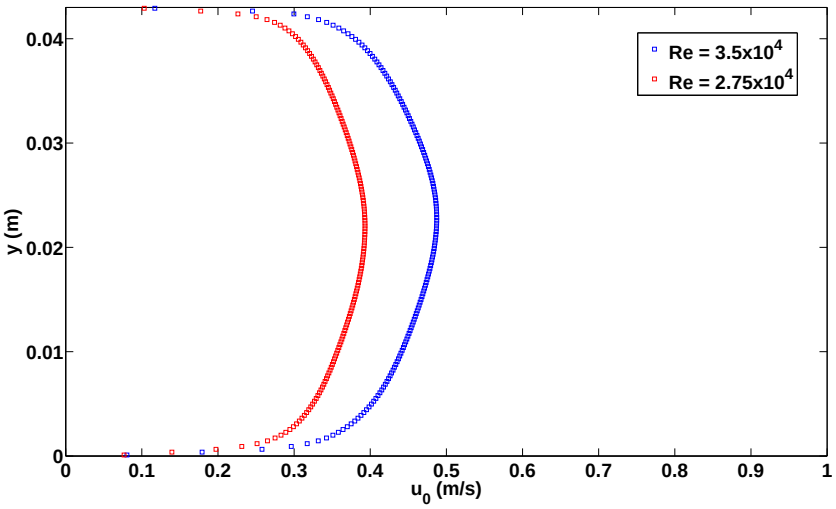

Figura 4: **Profiles of the mean velocities.**

For this type of flow the law of the wall is valid and the shear velocity $u_{*,0}$ was then determined by fitting the experimental data in the logarithmic region ($70 < y^+ < 200$), and by considering a hydraulic smooth regime (Schlichting and Gersten, 2003).

Figures 5a and 5b present the log-normal profiles of the mean velocities for top e bottom walls for the two Reynolds numbers. The ordinate is in linear scale and corresponds to mean velocities normalized by the shear velocity, u_0^+. The abscissa is in logarithmic scale and represents the vertical distance from the channel walls (bottom or top) normalized by the viscous length, y^+.

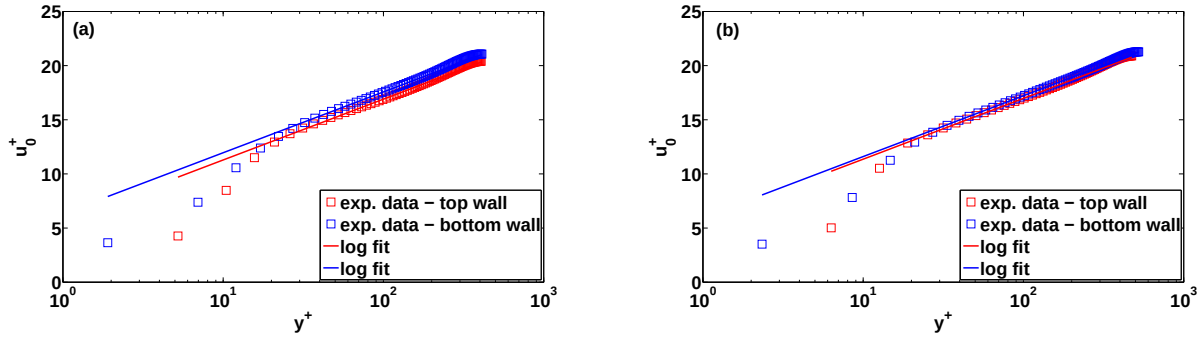

Figura 5: **Velocity profiles: (a) Re = 2.75×10^4; (b) Re = 3.5×10^4.**

Figure 6 presents the Reynolds stress profiles (for both Reynolds numbers) in dimensionless form, y/H_{eff} versus $-\overline{u_0'v_0'}/(u_{*,0}^2)$. For the upper and bottom parts of the profiles, the normalization was made by using the respective unperturbed shear velocities for each Reynolds number. Table 1 presents the unperturbed shear velocities. The profiles are as expected for channel flows (Schlichting and Gersten, 2003).

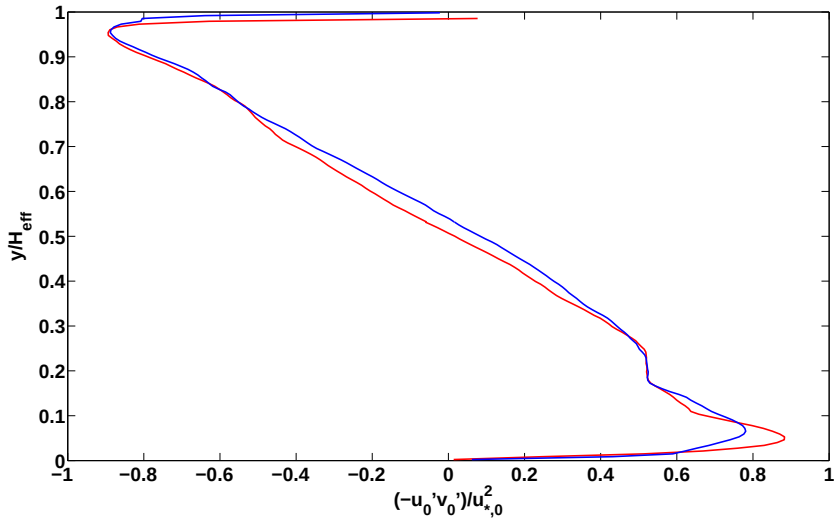

Figura 6: **Profiles of the xy component of the Reynolds stress in dimensionless form. The red line corresponds to Re = 2.75×10^4 and the blue line to Re = 3.5×10^4**

Tabela 1: **Unperturbed shear velocities for each Reynolds number**

Re		$u_{*,0}(m/s)$
2.75×10^4	top wall	0.0193
	bottom wall	0.0187
3.5×10^4	top wall	0.0233
	bottom wall	0.0229

3.2 Perturbed flow

The same flow rates were used for the flow over the ripple. In the following we present some results for the central part of the ripple (crest region), with Re = 2.75×10^4.

Figure 7 presents the longitudinal and vertical components of mean velocity profile for different longitudinal positions. The vertical coordinate y_d, given by $y_d = y - h$, where h is the hill's local height, is the proper coordinate close to the bottom wall because, in the lower region, close to the ripple, the ripple surface is the reference.

In Fig. 7a we observe in this region an increase of u as the flow approaches the ripple crest, what is expected from the mass conservation. Fig. 7b shows that v increases from zero at the ripple surface, reaches a maximum and decrease to zero as y_d approaches the upper wall. For every longitudinal position the maximum occurs between 0.9 and 1.6 mm. Franklin and Ayek (2013) found, for a bedform of triangular shape, that toward the crest the maximum of the vertical component becomes closer to the ripple surface ($y_d \approx 2mm$). The explanation for this difference lies in the relatively small curvature of our bedform.

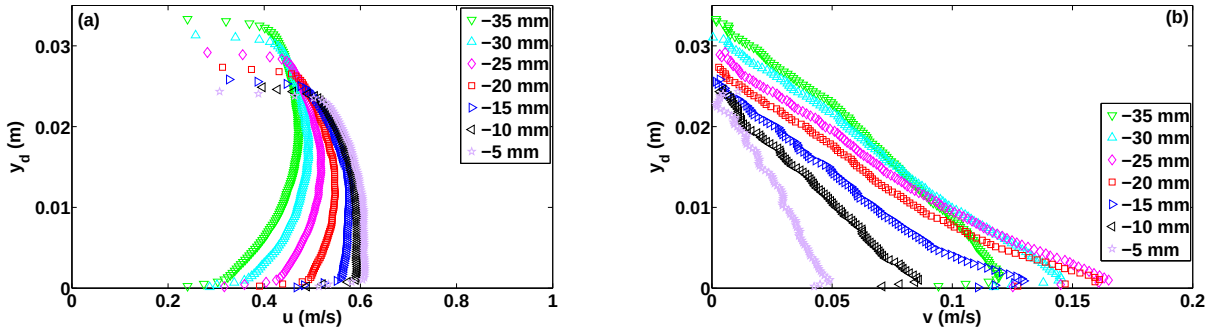

Figura 7: **Velocity profiles for Re = 2.75×10^4 : (a) longitudinal velocities; (b) vertical velocities.**

Having as reference the solid walls, we can define the perturbation field as the difference between the flow over the ripple and that over a flat wall (Jackson and Hunt, 1975). For the mean velocity $\Delta\mathbf{V}(y_d) = \mathbf{V}(y_d) - \mathbf{V}_0(y_d)$, where $\mathbf{V}_0(y_d) = u_0(y)\hat{i}$ and u_0 is obtained from the law of wall. Figure 8 shows some perturbation profiles of the mean velocity along the ripple.

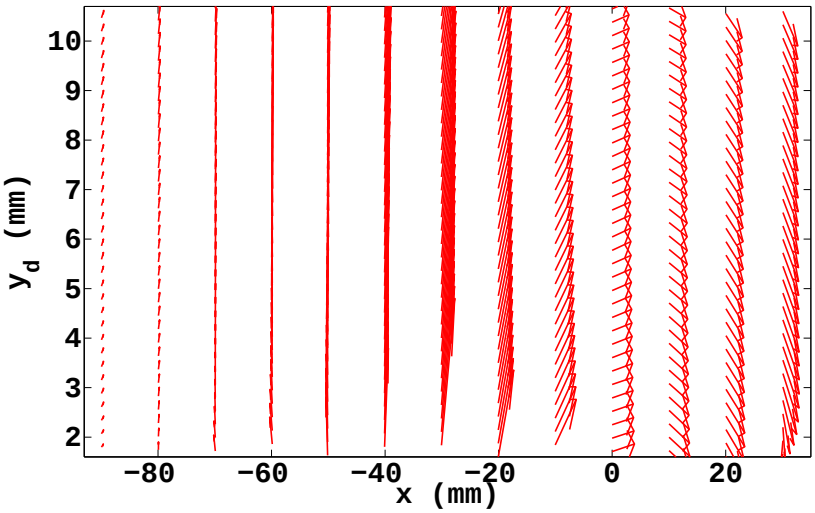

Figura 8: **Perturbation profiles of the mean velocities $\Delta\mathbf{V}$.**

Some profiles of the xy component of the Reynolds stress upstream the crest in dimensionless form, y_d^+ versus $-\overline{u'_\theta v'_\theta}/(u^2_{*,0})$, where $y_d^+ = y_d u_{*,0}/\nu$, are presented in Fig. 9a. Here u_θ and v_θ are respectively the aligned and perpendicular components of the mean velocity with respect to the hill surface, and u'_θ and v'_θ are the longitudinal and vertical components of the velocity fluctuation, respectively. The figure shows that the Reynolds stress is perturbed in the $50 < y_d^+ < 250$ region, which corresponds to the overlap sublayer of the unperturbed boundary layer (Schlichting and Gersten, 2003). Fig. 9a also shows that, longitudinally, the perturbation of $-\overline{u'_\theta v'_\theta}$ decreases near the crest. Figure 9b presents the longitudinal evolution of the maximum of the $-\overline{u'_\theta v'_\theta}$. For both Re, the highest values are reached in the 50 mm $< x <$ 40 mm region, although other two pronounced peaks appears, whose reasons are still under investigation. Both curves have the same behaviour, $(-\overline{u'_\theta v'_\theta})_{max}$ decreases and remains stable in the -10 mm $< x <$ 0 region. It is possible to see four curves in the -40 mm $< x <$ -20 mm region, the reason for that is, in this interval we have the overlap of two parts of the experiment, and we have chosen to maintain this to show that the behaviour is well preserved.

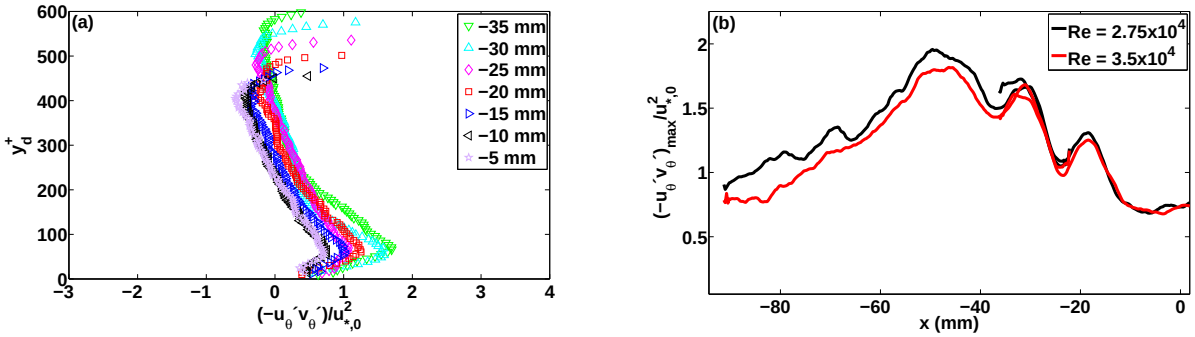

Figura 9: **Reynolds stresses: (a) profiles, for $\mathrm{Re} = 2.75 \times 10^4$; (b) longitudinal evolution of the maxima of Reynolds stresses.**

We computed the production term of turbulent kinetic energy ($-\overline{u'_\theta v'_\theta}\partial u_\theta/\partial y_{d,\theta}$) , and the values are presented in Fig. 10. Here $y_{d,\theta}$ is the displaced coordinate perpendicular to the hill surface. Downstream the crest we can see a region of production confined near the hill surface, what is expected due the relatively small curvature of the bedform.

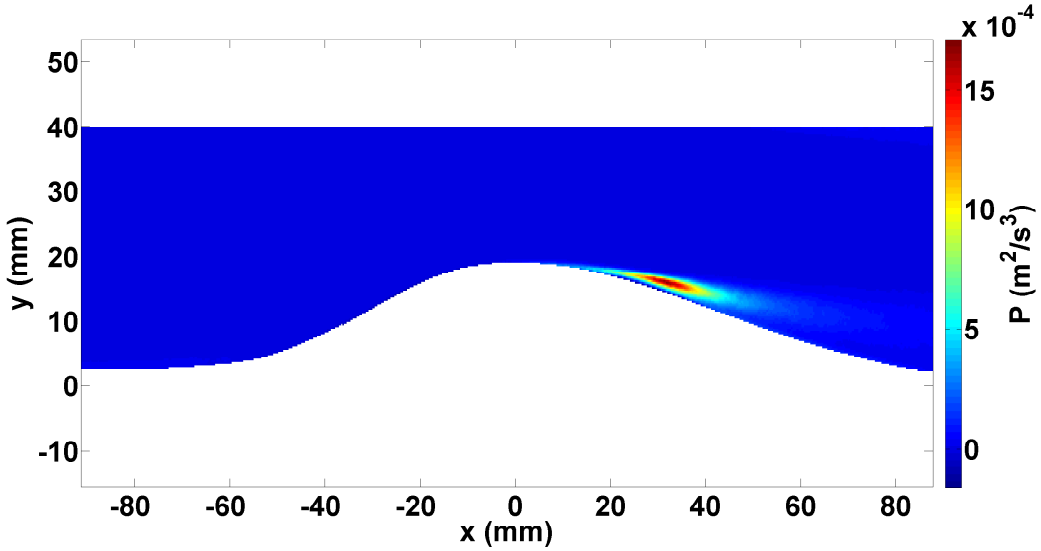

Figura 10: **Production of turbulent kinetic energy.**

4. CONCLUSION

This paper presented some experimental results on the perturbation of a liquid turbulent boundary layer by a two-dimensional ripple in the hydraulic smooth regime. We encountered some usual characteristics of a fully-developed turbulent channel flow, such as the logarithmic region for both walls and the typical profiles of the xy component of the Reynolds stress. We presented some results about the velocities upstream the ripple crest. For the u component of the mean velocity, we observed an increase as the flow approaches the ripple crest, and for the vertical component v, the maxima are between 0.9 and 1.6 mm. The results for the longitudinal component are in agreement with previous studies, even if the bedform shapes differ. For the vertical component, the small curvature of our bedform explains the difference in results. We also presented here the xy component of the Reynolds stress upstream of the ripple crest, and is possible to see that the profile is perturbed in the $50 < y_d^+ < 250$ region, which correspond to the overlap region of the unperturbed boundary layer. Additionally we presented the longitudinal behaviour of the maximum for the Reynolds stress. Finally, we showed the turbulence kinetic energy production.

5. ACKNOWLEDGEMENTS

The authors are grateful to FAPESP (contract numbers 2014/08943-4 and 2012/19562-6).

6. REFERENCES

Belcher, S.E. and Hunt, J.C.R., 1998. "Turbulent flow over hills and waves". *Annual Review of Fluid Mechanics*, Vol. 30, No. 1, pp. 507–538.

Franklin, E.M., 2010. "Initial instabilities of a granular bed sheared by a turbulent liquid flow: length-scale determination". *Journal of the Brazilian Society of Mechanical Sciences and Engineering*, Vol. 32, No. 4, pp. 460–467.

Franklin, E.M., 2011. "Nonlinear instabilities on a granular bed sheared by a turbulent liquid flow". *Journal of the Brazilian Society of Mechanical Sciences and Engineering*, Vol. 33, No. 3, pp. 265–271.

Franklin, E.M., 2012. "Linear and nonlinear instabilities of a granular bed: Determination of the scales of ripples and dunes in rivers". *Applied Mathematical Modelling*, Vol. 36, No. 3, pp. 1057–1067.

Franklin, E.M. and Ayek, G.A., 2013. "The perturbation of a turbulent boundary layer by a two-dimensional hill". *Journal of the Brazilian Society of Mechanical Sciences and Engineering*, Vol. 35, pp. 337–346.

Franklin, E.M. and Charru, F., 2009. "Morphology and displacement of dunes in a closed-conduit flow". *Powder Technology*, Vol. 190, No. 1-2, pp. 247–251.

Jackson, P.S. and Hunt, J.C.R., 1975. "Turbulent wind flow over a low hill". *Quarterly Journal of the Royal Meteorological Society*, Vol. 101, No. 430, pp. 929–955.

Schlichting, H. and Gersten, K., 2003. *Boundary-layer theory*. Springer Science & Business Media.

7. RESPONSIBILITY NOTICE

The author(s) is (are) the only responsible for the printed material included in this paper.